

Cold-Cavity Thresholds of Microdisks With Uniform and Nonuniform Gain: Quasi-3-D Modeling With Accurate 2-D Analysis

Elena I. Smotrova, *Student Member, IEEE*, Alexander I. Nosich, *Fellow, IEEE*, Trevor M. Benson, *Senior Member, IEEE*, and Phillip Sewell, *Senior Member, IEEE*

Abstract—An electromagnetic analysis of thin-disk semiconductor resonators with uniform and nonuniform gain regions is presented. A “cold-cavity-with-gain” Maxwellian formulation, including accurate boundary and radiation conditions, is considered as an eigenvalue problem, for the real-valued parameters of frequency and threshold material gain. Although the well-known approximate effective-index method is used to reduce a three-dimensional (3-D) field problem to a two-dimensional (2-D) one, a rigorous formulation of the latter is retained. A quasi-3-D feature is provided through full account of the multiple-wave nature and dispersion of the effective index. Results obtained quantify the ultralow thresholds of the whispering-gallery modes and show the advantage of a ring-shaped gain region.

Index Terms—Microdisk, threshold, whispering gallery modes.

I. INTRODUCTION AND MOTIVATION

MICRODISK lasers were demonstrated in the 1990s as extremely compact and ultralow-threshold sources of light [1]–[3]. Lasing in 1–10- μm diameter GaAs disks containing quantum wells was achieved initially with a photopump and then with the injection of current. Later, etched microdisk lasers with quantum cascades [4], boxes [5], and dots [6] were reported. It was realized at an early stage that the disk lasing modes were the quasi-whispering-gallery (WG) ones whose optical field traveled along the rim and experienced almost total internal reflection. At first, the description of these modes was done analytically using asymptotic techniques [1], [7]–[9]. Here, the three-dimensional (3-D) problem for a finite-thickness disk was approximately reduced to the two-dimensional (2-D) one, i.e., to a circular resonator in the plane of the disk, with the aid of the effective-index approach previously developed for dielectric waveguides and vertical-cavity surface-emitting lasers (VCSELs) [10]. The assumption that the modal field vanished at the disk rim (as for a classical WG mode) was found good enough to explain the measured lasing frequencies. To estimate quality factors (Q-factors), conformal mapping of the circle to the planar geometry was used, with the subsequent consideration of tunneling via the Wentzel–Kramér–Brillouin (WKB) approximation.

Manuscript received October 14, 2004, and October 22, 2004; revised June 13, 2005, and June 16, 2005. This work was supported by the EPSRC-UK under Grant GR/S60693/01P, and by the Royal Society under Grant IJP-2004/R1-FS. The work of E. I. Smotrova was supported by INTAS-EU via a Ph.D. fellowship.

E. I. Smotrova and A. I. Nosich are with the Institute of Radio-Physics and Electronics of the National Academy of Sciences of Ukraine (IRE NASU), Kharkov 61085, Ukraine (e-mail: elena_smotrova@yahoo.com).

T. M. Benson and P. Sewell are with the George Green Institute for Electromagnetics Research, University of Nottingham, Nottingham NG7 2RD, U.K.

Digital Object Identifier 10.1109/JSTQE.2005.853848

This approach demonstrated that the WG mode Q-factors exponentially depend on frequency. It should be noted, however, that a simplified assumption about the exponential decay of the optical field outside of the disk is incorrect. Mathematically, if the frequency is real-valued, a time-harmonic electromagnetic field obeys the radiation condition and therefore decays only as $O(R^{-1})$ in the 3-D case or as $O(r^{-1/2})$ in the 2-D one, where $\mathbf{R} = \{r, \varphi, z\}$. If the frequency ω is complex-valued, as in eigenfrequency problems (see Appendix II), then there is no decay at all, as the modal field *a priori* diverges at infinity as $O(e^{|\text{Im } \omega| R/c} R^{-1})$ or $O(e^{|\text{Im } \omega| r/c} r^{-1/2})$, where c is the velocity of light.

The analytical approach of [7]–[9] is not applicable to a cavity with a more complicated shape, or to nonuniform gain or 3-D problems. Therefore, the finite-difference time-domain (FDTD) numerical method was used in [11] for the full 3-D-disk problem and, in [12], for the 2-D models. Commercial FDTD codes are more and more attractive today as flexible and ready-to-use simulation tools. Note, however, that so far an FDTD study of an *open resonator* entails severe difficulties in how to limit infinite host space and then mesh it properly [13]. Well-known sources of errors entering FDTD solutions are the staircasing of the curved material boundaries and the reflections from the virtual boundary of the computational window [14]. Additionally, FDTD is time and memory expensive even for simple geometries. Therefore, a suggestion of [15], [16] to consider microdisk lasing modes with an integral equation (IE) approach was a step in the right direction. However, it was not realized there.

In the aforementioned papers, the problem studied was that of calculating the natural modes of the *passive* open resonators. Once the complex-valued natural frequencies were found, it was stated that those with the largest Q-factors (i.e., the smallest values of $\text{Im } \omega$) corresponded to the lasing modes. It is easy to see that in this way the lasing phenomenon is not addressed directly. A complex-frequency eigenvalue problem can characterize only one of two basic features of lasing, namely, the discrete frequency spectrum. Another one, i.e., the specific value of threshold gain needed to force a mode to become lasing, is not included in this formulation, although sometimes researchers seek the value of the gain parameter, say γ , that brings the function $\text{Im } \omega(\gamma)$ to zero. It is also worth mentioning that the FDTD method is not applicable directly to eigenvalue problems; instead, it implies placing a pulsed source inside a cavity, studying the transient response, and eventually extracting the natural frequencies and Q-factors from such a response.

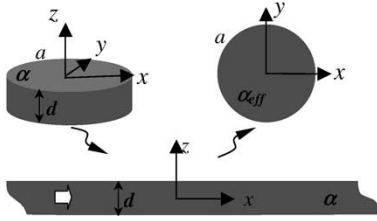


Fig. 1. 3-D geometry of a semiconductor circular disk microresonator and relevant problems of reduced dimensionality.

Therefore, in [17] we proposed the *Lasing Eigenvalue Problem* (LEP), specifically tailored to extract not only frequencies but also threshold gains from nontrivial solutions to the disk natural-field problem. In the present paper, we extend this work to accurately account for the effective-index dispersion and study the effect of gain nonuniformity on the lasing thresholds. Such a study is valuable for a better insight into the fundamental optical wavelength-scale phenomena that occur in microcavity lasers.

In Section II, we consider, both analytically and numerically, a LEP for the 2-D model of microdisk laser with uniform gain. Unlike previous works, we keep a rigorous 2-D formulation and take into account, in comprehensive manner, the multivalued character and the dispersion of the disk effective index. Section III presents a comparison of our results with the experimental data of [5]. In Section IV, we study spectra and thresholds for disk lasers with nonuniform gain and show ways of controlling the threshold in such cavities. Conclusions are presented in Section V. For convenience, Appendix I contains the essentials of the effective-index approach used to reduce dimensionality of the thin-disk problem. To help with general mathematical background, Appendix II reviews the basics of the eigenfrequency problems for the complex-valued natural frequencies and generalized natural modes of open resonators, and gives a comparison with the more adequate “cold-cavity” LEP model of lasing.

II. MICRODISK LASER WITH UNIFORM GAIN

Fig. 1 shows the geometry of a microdisk cavity. Suppose that disk of the thickness d and radius a is nonmagnetic and isotropic, and has real-valued refractive index α ; the host medium is vacuum. The electromagnetic field is assumed to have the time dependence $e^{-i\omega t}$; then free-space wavenumber is $k = \omega/c = 2\pi/\lambda$, where λ is wavelength.

Assume that we have already reduced the problem to the 2-D model as discussed in Appendix I. Then we can treat either of two polarization states separately, with the aid of one function U (i.e., E_z or H_z component in the disk plane). The LEP statement implies (see Appendix II) that U has to satisfy the 2-D Helmholtz equation (A8) where, if $r < a$, the coefficient α_{eff} is replaced with the complex-valued parameter $\nu = \alpha_{\text{eff}(q)}^{H,E} - i\gamma$; otherwise, $\alpha_{\text{eff}} = 1$. Here, the effective index is associated with the q th guided wave of a slab of the same thickness as the disk ($1 < \alpha_{\text{eff}(q)}^{H,E} < \alpha$) and satisfies (A11). In Section II, we assume that $\gamma > 0$ is constant, i.e., the gain is uniform across the disk, while two cases of nonuniform gain will be analyzed in Section IV. At

the disk rim, the transparency conditions (A12) hold, with $\beta^H = \nu^{-2}$ and $\beta^E = 1$. The condition of the local energy finiteness is given by (A13). Thanks to the real-valued k , U obeys the usual 2-D radiation condition (A15) and does not diverge at infinity.

Considering the LEP, we look for two real numbers, $\kappa = ka$ and γ . The first of them is the normalized lasing frequency, while the second is the threshold material gain. Here, we stress that the value of the lasing threshold γ extracted from the LEP cannot be simply derived from the Q-factor (or decay rate, $\text{Im } k$) for the eigenfrequency problem, because ν enters the LEP not only as a product with k but also independently.

The circular symmetry leads to the separation of variables:

$$U(r, \varphi) = F(r)\Phi(\varphi). \quad (1)$$

Substituting this into (A8), we can see that

$$\frac{d^2 F}{dr^2} + \frac{1}{r} \frac{dF}{dr} \left(\nu^2 r^2 - \frac{m^2}{r} \right) F = 0, \quad \frac{d^2 \Phi}{d\varphi^2} + m^2 \Phi = 0 \quad (2)$$

where, thanks to the periodicity in φ , $m = 0, 1, 2, \dots$. Taking into account (A13) and (A15), we conclude that

$$U(r, \varphi) = \begin{cases} AJ_m(\kappa\nu r/a), r < a \\ BH_m^{(1)}(\kappa r/a), r > a \end{cases} \begin{cases} \cos \\ \sin \end{cases} m\varphi \quad (3)$$

where J_m and $H_m^{(1)}$ are the Bessel and Hankel functions, respectively. Note that, mathematically, any lasing mode field is a stationary (i.e., standing) wave; there are no separate clockwise and counterclockwise propagating waves.

Thus, all modes in the circular cavity split into independent families according to the azimuth index m , and those with $m > 0$ are twice degenerate. For each family, the conditions (A12) generate a complex-valued characteristic equation:

$$J_m(\kappa\nu)H_m^{(1)}(\kappa) - \beta^{E,H} \nu J_m'(\kappa\nu)H_m^{(1)}(\kappa) = 0 \quad (4)$$

whose roots are eigenvalues. To number them, we introduce the second index n , which will correspond to the number of the field variations in the radial direction. Furthermore, we recall that the effective-index method introduces a third index q (see Appendix I), so that the roots are denoted as $(\kappa_{mnq}, \gamma_{mnq})$, where $m, q \geq 0, n \geq 1$. Note that reduction of (4) to the “no-leakage” form (as in [1]–[9]), $J_m(\kappa\nu) = 0$ or $J_m'(\kappa\nu) = 0$, yields zero thresholds.

For accurate computation of the lasing spectra and thresholds in realistic semiconductor microdisks, we applied a two-parameter secant-type iterative method (see Fig. 2). To provide a quasi-3-D feature to our analysis, we accurately accounted for the dispersion of the effective index as one of the roots of the corresponding dispersion (A11). The cylindrical functions in (4) were calculated to machine precision with forward and backward recursion [18].

As initial guess we took the following expressions:

$$\kappa_{mn}^{H,E} \approx \frac{\pi}{2\alpha} \left(m + 2n \mp \frac{1}{2} \right) \quad (5)$$

and also

$$\gamma_{mn}^{H,E} \approx \frac{\pi}{2\kappa_{mn}^{H,E}} \ln \left(\frac{\alpha + 1}{\alpha - 1} \right), \quad \text{if } \kappa_{mn}^{H,E} \gg m \quad (6)$$

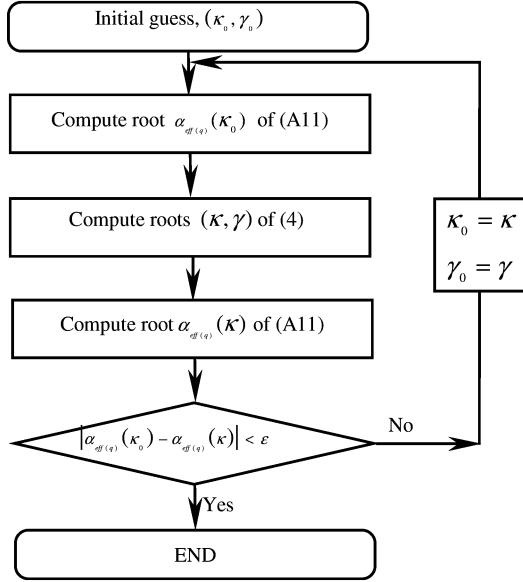


Fig. 2. Adaptive computational algorithm.

or

$$\gamma_{mn}^{H,E} \approx C_{H,E} e^{-2m \ln(2m/\kappa_{mn}^{H,E})}, \quad \text{if } m/\alpha \ll \kappa_{mn}^{H,E} \ll m$$

$$C_E = \frac{e}{4\kappa_{mn}^E \alpha} \left(\frac{2m}{e\kappa_{mn}^E} \right)^3$$

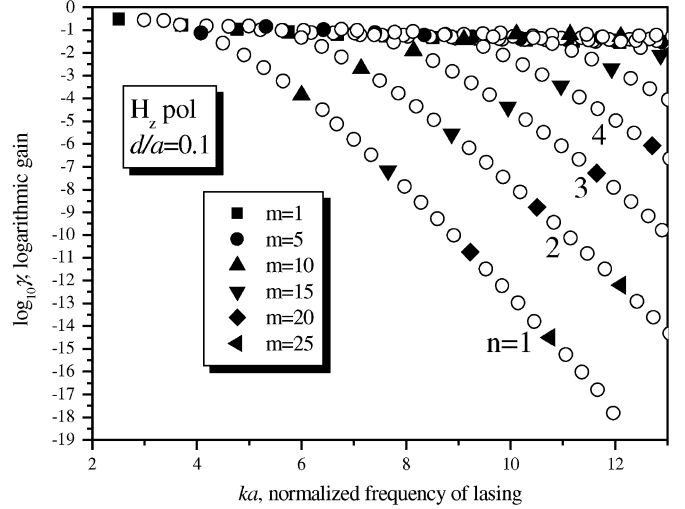
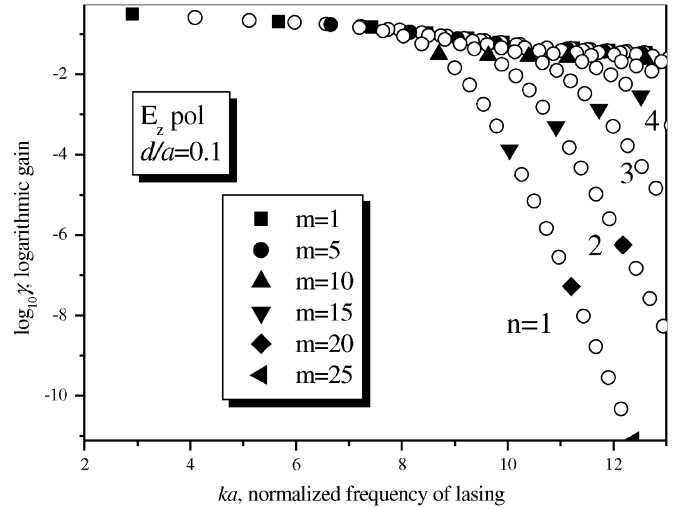
$$C_H = \frac{\alpha \kappa_{mn}^H e}{4 \left[m + (\kappa_{mn}^H)^2 + m^2 \alpha^2 \right]} \left(\frac{2m}{e\kappa_{mn}^H} \right)^3. \quad (7)$$

Note that (7) quantifies exponentially small thresholds of the WG modes. To derive these formulas from (4), we used the asymptotic expressions for the cylindrical functions [18].

The lasing spectra and thresholds in a GaAs microdisk of the thickness $d = 0.1a$, computed with account of the dispersion of effective indices of two principal slab waves TE_0 and TM_0 , are presented in Figs. 3 and 4, respectively.

The plane (κ, γ) happens to be inhabited by the LEP eigenvalues in a nonuniform manner. One can clearly see the hyperbolas $\gamma \approx \text{const}/\kappa$ given by (6) and “saturated” with modes of all the m th families. These modes have very high thresholds, $\gamma > 0.01$. Above that curve, there are no lasing modes. In contrast, in each family with $m > \alpha_{\text{eff}}$, the modes which have $\kappa < m$ but still $\kappa > m/\alpha_{\text{eff}}$ display drastically smaller values of γ . These values are close to (7) and smaller for larger m , as predicted. Therefore, below the hyperbola mentioned the eigenvalues form inclined “layers,” with each “layer” corresponding to a certain radial index n . The effect of the index dispersion is seen in the varying inclination of “layers” as compared to [17, Figs. 2 and 3].

Thus, the modes in a circular cavity do not automatically show the “whispering” property, i.e., do not have $\gamma \approx e^{-\text{const}\kappa}$ as given by (7). This is true only for the modes (not necessarily with $n = 1$) that experience quasi-total internal reflection at the rim of the cavity [8], [9]. Still, the modes having single variation in radius ($n = 1$) form the “aristocracy” of the WG modes—they inhabit the lowest-threshold “layer.” A compar-

Fig. 3. Lasing spectra and threshold gains for the H_z -polarized modes of the families $(H_z)_{mn0}$ in a GaAs disk, $\alpha = 3.374$ and $d/\alpha = 0.1$.Fig. 4. The same as in Fig. 3 for the modes of the families $(E_z)_{mn0}$.

ison of Figs. 3 and 4 shows the effect of the smaller effective index, for the same disk and index q , of the E_z -polarized modes than of the H_z -polarized ones. If, e.g., $\lambda_0 = 1.55 \mu\text{m}$ and $d = 200 \text{ nm}$, then $\alpha_{\text{eff}(0)}^E = 1.31$ and $\alpha_{\text{eff}(0)}^H = 2.64$. Therefore, the E_z -modes have only a small chance for lasing unless κ is large enough. Near-field portraits of some modes are given in Figs. 5 and 6. They demonstrate a relative field confinement for the WG modes and a relative leakage for the non-WG ones.

Similar data were computed for the other effective indices with $q > 0$. They showed considerable blueshifts of the lasing frequencies and higher thresholds due to the smaller effective contrast (see Appendix I).

III. VERIFICATION OF THE THEORY

To estimate the validity of the new results obtained, we have compared them with the experimentally measured lasing spectra of a GaAs microdisk cavity with InAs quantum boxes that can

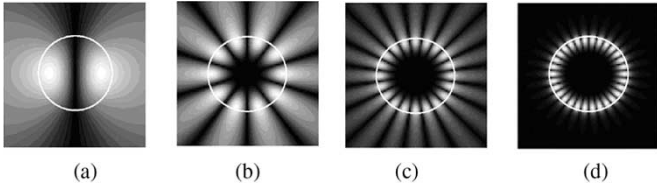


Fig. 5. Near E-field portraits for the E_z -polarized lasing modes of a GaAs microdisk, $\alpha = 3.374$ and $d/\alpha = 0.1$. (a) $(E_z)_{1,1,0}$, $ka = 2.9$, $\gamma = 0.23$, $\alpha_{\text{eff}} = 1.01$; (b) $(E_z)_{5,1,0}$, $ka = 6.65$, $\gamma = 0.17$, $\alpha_{\text{eff}} = 1.12$; (c) $(E_z)_{10,1,0}$, $ka = 8.7$, $\gamma = 3.1 \times 10^{-2}$, $\alpha_{\text{eff}} = 1.46$; (d) $(WGE_z)_{15,1,0}$, $ka = 10.03$, $\gamma = 1.33 \times 10^{-4}$, $\alpha_{\text{eff}} = 1.86$.

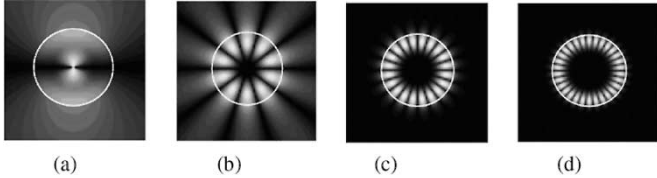


Fig. 6. The same as in Fig. 5 for the H_z -polarized lasing modes. (a) $(H_z)_{1,1,0}$, $ka = 2.5$, $\gamma = 0.29$, $\alpha_{\text{eff}} = 1.55$; (b) $(H_z)_{5,1,0}$, $ka = 4.08$, $\gamma = 7.4 \times 10^{-2}$, $\alpha_{\text{eff}} = 1.98$; (c) $(WGH_z)_{10,1,0}$, $ka = 5.99$, $\gamma = 1.4 \times 10^{-4}$, $\alpha_{\text{eff}} = 2.36$; (d) $(WGH_z)_{15,1,0}$, $ka = 7.65$, $\gamma = 6.8 \times 10^{-8}$, $\alpha_{\text{eff}} = 2.58$.

be found in [5, Fig. 2]. The corresponding photoluminescence curve is shown at the bottom of our Fig. 7, with the original notations and mode indices from [5].

At the top of the figure we show the same strip, in frequency, on the (κ, γ) plane, with the eigenvalues computed by our model for several $\alpha_{\text{eff}}^{E,H}(\kappa)$. A comparison reveals that the WG modes $(H_z)_{23,1,0}$ to $(H_z)_{26,1,0}$ were identified in [5] quite accurately. However, other modes that go lasing in the experimental cavity are identified here differently from [5]; namely, they are the $(E_z)_{22,1,0}$ to $(E_z)_{25,1,0}$ ones from the second WG-mode “layer.” Further, one can notice that experimental spikes are grouped in pairs, which is explained by the removal of the double degeneracy of the disk modes due to the surface roughness. This supposition is supported by the photo of the microdisk [5, Fig. 1] that shows roughness of some 20-nm scale and a large nonsymmetric pedestal. Moreover, a closer inspection of the experimental curve reveals small peaks (marked \times) at the very onset of lasing. Our theory readily suggests that these modes are the $(H_z)_{20,2,0}$, $(H_z)_{21,2,0}$, and $(E_z)_{21,2,0}$ ones. All the other modes were apparently below threshold with the pump power used in the experiment. We stress that to obtain this agreement we had to account for the dispersion of the effective indices involved. Note that the disk in [5] was rather thick, with $d/a = 0.17$. Comparisons with the other published data for the lasing frequencies of the thinner disks (not shown here) demonstrated even better agreement with our simulations.

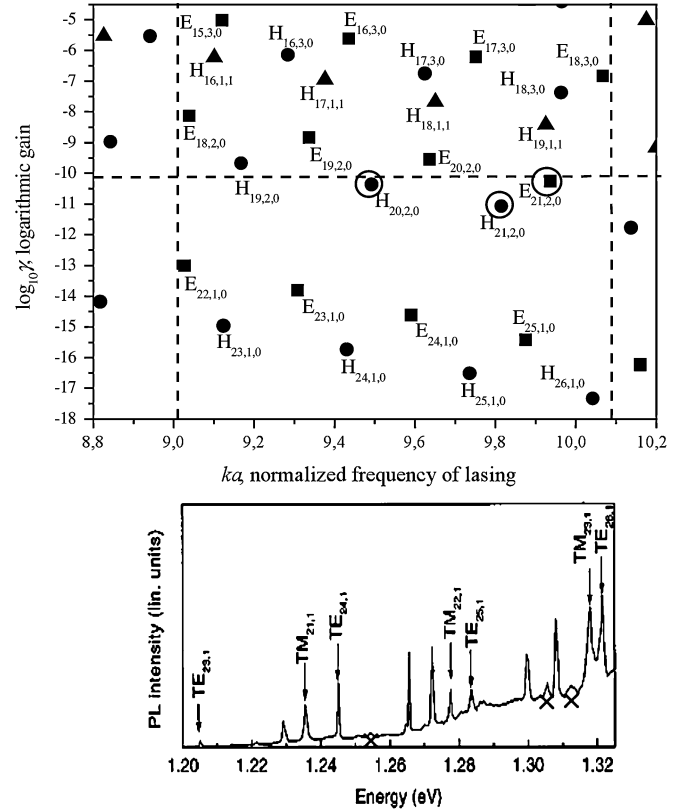


Fig. 7. Comparison of the results computed with the model of this paper (upper part) and the lasing spectrum measured in [5] (lower insert). GaAs/InAs microdisk parameters: $\alpha = 3.374$, $\alpha = 1.5 \mu\text{m}$, $d = 0.25 \mu\text{m}$.

IV. MICRODISK LASERS WITH NONUNIFORM GAIN

Injection lasers are frequently designed as stacked structures where a microdisk cavity is sandwiched between the substrate and metal contacts [11]. The density of injected carriers, and, hence, the material gain, can then have greater values in the center than at the rim. Furthermore, it is possible to design lasers with patterned contacts to produce nonuniform gain in order to tailor the lasing characteristics [19]. To simulate these nonuniform gain features, we shall assume that the gain γ is step-like, i.e., uniform inside a circle of radius $b < a$ and zero outside. On using an additional transparent boundary condition at $r = b$, the “cold-cavity-with-gain” characteristic equation is derived as (see (8) at the bottom of the page), where the new parameter is $\delta = b/a$. Fig. 8 illustrates the $(H_z)_{mn0}$ -type mode spectra and thresholds for a circular-shaped active area having a radius half that of the disk.

The comparison of this figure with the similar one for a uniform-gain GaAs disk (Fig. 3) shows that the modes keep their location in frequency. However, they have thresholds higher by

$$\det \begin{bmatrix} H_m^{(1)}(\kappa) & -J_m(\kappa\alpha) & -H_m^{(1)}(\kappa\alpha) & 0 \\ H_m^{(1)}(\kappa) & -\beta\nu J_m'(\kappa\alpha) & -\beta\nu H_m^{(1)}(\kappa\alpha) & 0 \\ 0 & J_m(\kappa\alpha\delta) & H_m^{(1)}(\kappa\alpha\delta) & -J_m(\kappa\nu\delta) \\ 0 & \beta\nu J_m'(\kappa\alpha\delta) & \beta\nu H_m^{(1)}(\kappa\alpha\delta) & -J_m'(\kappa\nu\delta) \end{bmatrix} = 0. \quad (8)$$

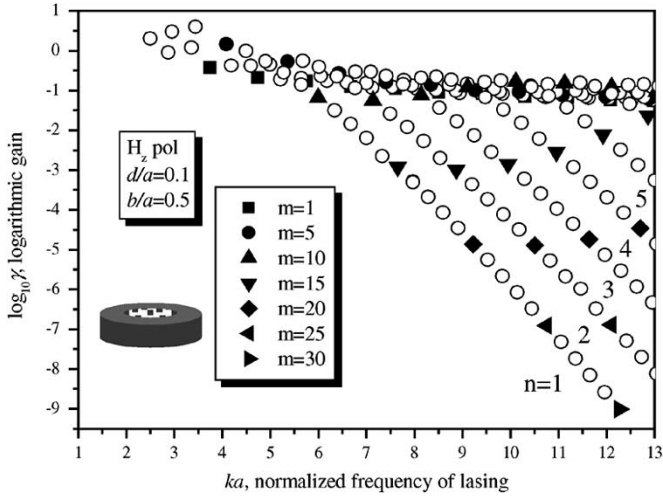


Fig. 8. Lasing spectra and threshold gains for the H_z -polarized modes of the families $(H_z)_{mn0}$ in a GaAs disk with circular gain extending to the half of disk radius., $\alpha = 3.374$ and $d/a = 0.1$.

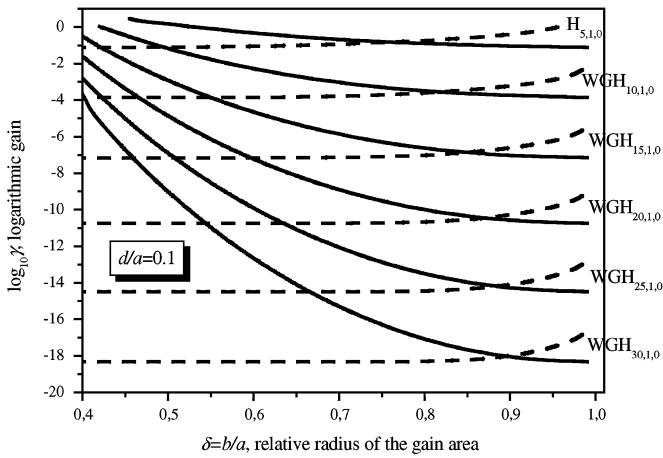


Fig. 9. Thresholds of the $(H_z)_{m1,0}$ modes in a GaAs disk with step-like gain on the relative outer (solid curves) and inner (dashed curves) radius of the gain area. $\alpha = 3.374$ and $d/a = 0.1$.

9 to 5 orders of magnitude. To make this effect clearer, Fig. 9 presents the dependences of the thresholds on the relative radius of gain area for the $(H_z)_{m1,0}$ modes.

Alternative designs of microdisk laser, i.e., with a ring gain along the rim, have been realized using an axicon-assisted hollow photopump beam [20] and a ring-shaped injection electrode [21]. For this type of configuration, our analysis leads to an equation like (8) where the values ν and α exchange places. Subsequent computation of the thresholds shows that now they are practically the same as for a disk with uniform gain, even if the ring-gain width is a small fraction of the disk radius. The larger the mode index m and the smaller the n , the narrower the allowable width of the pumped area. This can be seen in Fig. 9, where the plots of thresholds for the ring-gain disk are presented versus the relative radius of the gain area.

V. CONCLUSION

We have demonstrated that the cold-cavity thresholds of semiconductor microcavity lasers can be efficiently studied with a specialized eigenvalue problem, i.e., the LEP. Even the analysis of an approximate, effective-index-based, quasi-3-D LEP for a circular microdisk—if done accurately—brings valuable information. We have shown that in the plane (κ, γ) there are domains free of lasing modes. We have also quantified the most famous feature of microdisk lasers—the ultralow thresholds of the WG modes. This includes direct characterization of several effects: 1) disk modes display the WG character only if the condition of almost total internal reflection is satisfied, $\kappa_{mnq}^{E,H} < m < \alpha_{\text{eff}(q)}^{E,H} \kappa_{mnq}^{E,H}$; 2) $(H_z)_{mn0}$ modes have lower thresholds than their $(E_z)_{mn0}$ counterparts, thanks to the property that $\alpha_{\text{eff}(0)}^H > \alpha_{\text{eff}(0)}^E$; and 3) in larger and thicker disks, mode competition occurs, and the nearest higher order, in q , modes $(H_z)_{m1,1}$ have also to be considered.

The LEP is easily adaptable to microdisk laser configurations with nonuniform gain areas. We have shown that placing the active zone at the disk center, as typical for injection lasers, is catastrophic for the ultralow thresholds. In contrast, if the gain forms a ring along the disk edge, its width can be kept very small without raising the threshold. This effect leads to reduction of pump power—(see [20], [21]).

Our further goal is to study LEPs for more complicated shapes of microcavities using a boundary IE method [22].

APPENDIX I

REDUCTION OF DIMENSIONALITY

A. 3-D Formulation

The full 3-D frequency eigenvalue problem implies that we seek the natural frequencies k , which generate nontrivial fields $\{\mathbf{E}, \mathbf{H}\}$ solving, off the disk surface S , the set of *homogeneous Maxwell equations* with a piecewise-constant refraction index equal to α inside S and 1 outside:

$$\text{curl } \mathbf{E} = ikZ_0 \mathbf{H}, \quad \text{curl } \mathbf{H} = -ik\alpha^2 Z_0^{-1} \mathbf{E} \quad (\text{A1})$$

where $Z_0 = (\mu_0/\varepsilon_0)^{1/2}$ is free-space impedance. Additionally, *transparent boundary conditions* are satisfied on S

$$\mathbf{E}_{\text{tan}}^- = \mathbf{E}_{\text{tan}}^+, \quad \mathbf{H}_{\text{tan}}^- = \mathbf{H}_{\text{tan}}^+ \quad (\text{A2})$$

where the superscripts “ \pm ” refer to the limiting values of the functions from inside and outside the disk, respectively, and the subscript tan is for the field components lying tangential to S . Moreover, the electromagnetic energy must be locally integrable to prevent source-like field singularities:

$$\int_V [\alpha^2 \mathbf{E}^2(\mathbf{R}) + \mathbf{H}^2(\mathbf{R})] d\mathbf{R} < \infty, \quad V \subset (r, \varphi, z). \quad (\text{A3})$$

Further, we must also include a certain *condition at infinity* ($R \rightarrow \infty$). This plays a very important role and eventually defines the localization of eigenvalues. For example, if one is interested in the real-valued k , one can impose the Silver–Muller

radiation condition [23]

$$\lim_{R \rightarrow \infty} \{ \mathbf{E}(\mathbf{R}) - Z_0 \mathbf{H}(\mathbf{R}) \times \mathbf{R}/R \} = 0. \quad (\text{A4})$$

This is the electromagnetic vector analogue of the Sommerfeld condition known in the theory of scalar waves governed by the Helmholtz equation; it provides for the spherical-wave behavior and, in addition, eliminates nontransverse field components at infinity. One can equivalently write (A4) as a set of asymptotic requests:

$$\begin{aligned} e^{-ikR} \{ E_R, H_R \} &\sim 0, & E_\varphi &= Z_0 H_\theta \sim \frac{e^{ikR}}{R} \Phi_1(\varphi, \theta) \\ E_\theta &= -Z_0 H_\varphi \sim \frac{e^{ikR}}{R} \Phi_2(\varphi, \theta), & R &\rightarrow \infty. \end{aligned} \quad (\text{A5})$$

However, the Poynting theorem, applied to an eigenfunction $\{ \mathbf{E}, \mathbf{H} \}$ and its complex conjugate, leads to the conclusion that, independently of the geometry of the open resonator, real-valued eigenfrequencies do not exist. Therefore, to comply with the physical situation, it is necessary to admit complex values of k . Here, (A5) is convenient as it holds for any complex k .

Then the same Poynting theorem leads to the conclusion that the eigenvalues can be located only in the lower halfplane of the k -plane; i.e., each of them has a negative imaginary part for the selected time dependence (it would be positive if it were $e^{i\omega t}$). In this sense, they are *generalized eigenvalues* generating *generalized eigenfunctions* $\{ \mathbf{E}, \mathbf{H} \}$, whose components diverge at infinity as $O(e^{-\text{Im}kR}/R)$.

B. Effective-Index Reduction to 2-D Problem

For a thin disk, reduction of dimensionality from 3-D to 2-D is commonly based on the so-called effective-index model [1]–[9]. As we also use it here, we would like to present it from the mathematical point of view. In its core, one finds assumption that the field dependences on z and in-plane coordinates $\mathbf{r} = (r, \varphi)$ are separable in the whole space, e.g.,

$$E_z(\mathbf{R}) = V_E(z)U_E(r, \varphi), \quad H_z(\mathbf{R}) = V_H(z)U_H(r, \varphi). \quad (\text{A6})$$

In fact, this is incorrect because neither the boundary conditions on the whole disk surface S , nor the radiation condition at $R \rightarrow \infty$, is separable. However, such an assumption leads to independent differential equations for the functions of z and \mathbf{r} , commonly written as

$$\left[d^2/dz^2 + k^2\alpha^2 - k^2 \left(\alpha_{\text{eff}}^{E,H} \right)^2 \right] V_{E,H}(z) = 0 \quad (\text{A7})$$

where α turns 1 off the interval $|z| < d/2$ (see Fig. 1), and

$$\left[\frac{1}{r} \frac{\partial}{\partial r} \left(r \frac{\partial}{\partial r} \right) + \frac{1}{r^2} \frac{\partial^2}{\partial \varphi^2} + k^2 \alpha_{\text{eff}}^2 \right] U_{E,H}(r, \varphi) = 0 \quad (\text{A8})$$

where the refractive index $\alpha_{\text{eff}} = \alpha_{\text{eff}}^{H,E}$ is inside the cavity and one is outside. The boundary conditions for these functions depend on the polarization. For the functions of z , it is required

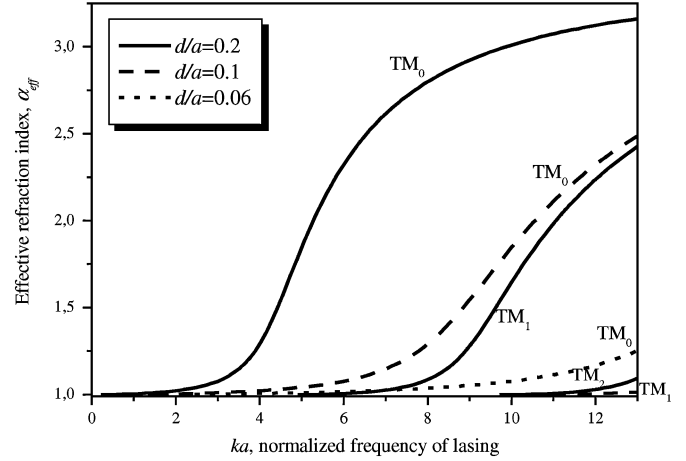


Fig. 10. Dispersion characteristics of the $(E_z)_q$ -waves of infinite dielectric slab made of GaAs. $\alpha = 3.374$.

that

$$\begin{aligned} V_{H,E}(\pm d/2 \mp 0) &= V_{H,E}(\pm d/2 \pm 0) \\ \frac{dV_{H,E}}{dz} \Big|_{z=\pm d/2 \mp 0} &= \beta^{H,E} \frac{dV_{H,E}}{dz} \Big|_{z=\pm d/2 \pm 0} \end{aligned} \quad (\text{A9})$$

where $\beta^H = \alpha^{-2}$ and $\beta^E = 1$.

Unfortunately, there is no “continuous” way to derive a one-dimensional (1-D) radiation condition at $z \rightarrow \pm\infty$ from the 3-D condition (A5). Anyway, to reproduce the outgoing wave propagation off the disk plane, one has to require that

$$V_{E,H}(z) \sim e^{ik(1-\alpha_{\text{eff}}^2)^{1/2}|z|}, \quad z \rightarrow \pm\infty. \quad (\text{A10})$$

Equations (A7), (A9), and (A10) form two familiar 1-D eigenvalue problems for the parameters α_{eff}^H and α_{eff}^E , which are identified as the normalized propagation constants of TE or TM waves of the infinite dielectric slab of thickness d and index α (Fig. 1). They are reduced to the transcendental equations for the even and odd waves, respectively,

$$\tan(pk d/2) = -\beta^{E,H} g p^{-1}, \quad \cot(pk d/2) = -\beta^{E,H} g p^{-1} \quad (\text{A11})$$

where $g^2 = (\alpha_{\text{eff}}^{E,H})^2 - 1$ and $p^2 = \alpha^2 - (\alpha_{\text{eff}}^{E,H})^2$.

For each type, there is a finite number $Q^{H,E} \geq 1$ of real-valued roots $\alpha_{\text{eff}(q)}^{H,E} : 1 < \alpha_{\text{eff}(q)}^{H,E} < \alpha$, corresponding to the guided waves ($q = 0, \dots, Q^{H,E} - 1$). The largest of them are of the TM_0 and TE_0 waves, respectively. The even (odd) value of the wave index indicates the symmetry (antisymmetry) of the wave field E_z or H_z with respect to the middle plane of the slab. Plots in Figs. 10 and 11 demonstrate the dependences of several effective indices on the frequency normalized by the disk radius, i.e., on $ka = kd(d/a)^{-1}$.

APPENDIX II 2-D EIGENVALUE PROBLEMS

A. Complex Frequency Eigenvalue Problem

On determining the set of effective indices $\alpha_{\text{eff}(q)}^{H,E}$ from (A11), one obtains independent 2-D problems for the in-plane fields

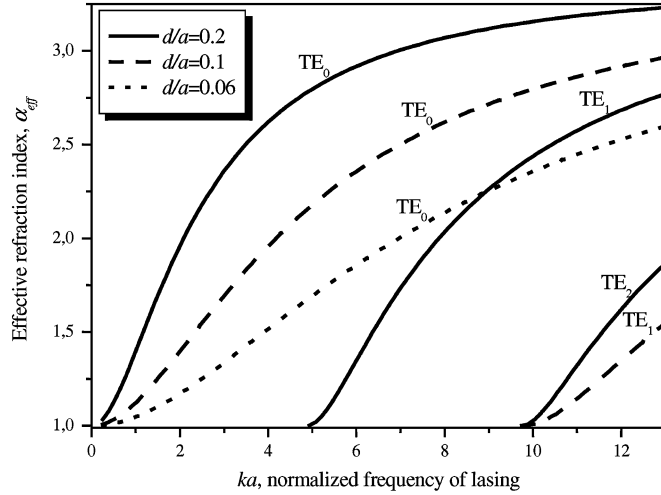


Fig. 11. The same as in Fig. 10 for the $(H_z)_q$ -waves.

$U_{H,E}(r, \varphi)$. Each problem involves (A8) with a piecewise constant refractive index and the 2-D conditions:

$$\begin{aligned} U^-(r, \varphi)|_L &= U^+(r, \varphi)|_L \\ \frac{\partial U^-(r, \varphi)}{\partial r} \Big|_L &= \beta^{H,E} \frac{\partial U^+(r, \varphi)}{\partial r} \Big|_L \end{aligned} \quad (\text{A12})$$

where superscripts “ \pm ” indicate the limiting values from inside and outside of the cavity contour L , respectively, $\beta^H = (\alpha_{\text{eff}}^H(q))^{-2}$, and $\beta^E = 1$. The field function must also satisfy the condition of the local energy finiteness:

$$\int_D (|kU|^2 + |\text{grad } U|^2) r dr d\varphi < \infty, \quad D \subset (r, \varphi) \quad (\text{A13})$$

and a condition at infinity valid for all complex k . Here, one meets the same problem as with function $V(z)$. In 3-D, we could simply take (A5) with complex-valued k thanks to the fact that the fundamental solution to the 3-D Helmholtz equation e^{ikR}/R was analytic in k . In 2-D, the same role is played by the outgoing Hankel function $H_0^{(1)}(kr)$, whose domain of analytic continuation is the Riemann surface of the function Lnk . Therefore, analytic continuation of the Sommerfeld condition to all complex k in 2-D has a more complicated form known as the Reichardt condition [24, Appendix]

$$U(r, \varphi) \sim \sum_{s=-\infty}^{\infty} a_s H_s^{(1)}(kr) e^{is\varphi}, \quad r \rightarrow \infty. \quad (\text{A14})$$

Thus, (A8) and (A12)–(A14) form a frequency eigenvalue problem in 2-D. Note, however, to arrive at it one has to make a series of inconsistent assumptions: 1) when imposing (A9) one neglects the finiteness of cavity radius; 2) when imposing (A12) one neglects the finiteness of the cavity thickness; and 3) when imposing (A10) and (A14) one admits completely different in-plane and off-plane field behavior. Other important observations are that: 4) effective index $\alpha_{\text{eff}}^{E,H}$ is a function of frequency; and 5) it has a discrete set of values corresponding to different slab waves.

Generally speaking, a 3-D problem is not equivalent mathematically to the “sum” of 1-D and 2-D problems just because there is no continuous transformation of 1-D or 2-D space into the 3-D space. Nevertheless, it is well known that the results obtained with the effective-index method are often more accurate than might be expected.

B. Lasing Eigenvalue Problem

Contrary to Appendix II-A, one may keep k real-valued and consider the eigenvalue problem in a modified formulation [17]. Assuming that it has been reduced to the 2-D model as discussed above, replace, in (A8), α_{eff} with $\nu = \alpha_{\text{eff}}^{H,E} - i\gamma$, if $r < a$, and 1 otherwise, where the new real-valued parameter appears—material gain, $\gamma > 0$. At the disk contour, impose the transparency conditions (A12) with complex ν , so that $\beta_{ef(q)f}^H = \nu^{-2}$ and $\beta_{\text{eff}}^E = 1$, and keep the condition (A13). Note, however, that thanks to the real-valued k , there is no need for condition (A14), and impose the usual 2-D Sommerfeld radiation condition:

$$U(r, \varphi) \sim (2/i\pi kr)^{1/2} e^{ikr} \Phi(\varphi) \quad r \rightarrow \infty. \quad (\text{A15})$$

We may now consider (A8), (A12), (A13), and (A15) modified in the above sense as a *lasing eigenvalue problem* (LEP). This means that, instead of looking for the real and imaginary parts of the modal wavenumber, as in the frequency eigenvalue problem, we are going to look for two real numbers, k and γ . The first of them is the lasing frequency while the second is the threshold material gain. Note that the value of gain in inverse centimeters can be found as $\gamma_0 = k\gamma$.

Of course, a LEP can be formulated in 3-D as well, as a lasing counterpart of (A1)–(A4), and account for the gain nonuniformity in vertical direction.

Thanks to the well-developed theory of the operator-valued functions, the basic properties of the lasing eigenvalues can be established even before their computation. The proof is based on the analytical regularization (see [25]), i.e., equivalent reduction of the considered boundary-value problem to a set of the Fredholm second-kind boundary IEs of Muller’s type [22], and the use of the operator extensions of the Fredholm theorems [26]. It is found that all $\gamma > 0$ and:

- 1) eigenvalues form a discrete set on the plane (k, γ) ;
- 2) each eigenvalue has finite multiplicity;
- 3) each eigenvalue depends on L, d , and α in piecewise-continuous or piece-analytic manner, and this property can be lost only if eigenvalues coalesce.

Note that one cannot simulate a spontaneous emission rate enhancement by studying a dipole radiating from an open cavity with gain. This is because if dipole frequency coincides with a lasing frequency, the enhancement is unlimited. To overcome this difficulty one has to introduce time dependence and saturation, i.e., nonlinearity.

ACKNOWLEDGMENT

The authors are grateful to A. V. Boriskin, S. V. Boriskina, and A. Vukovic for valuable discussions.

REFERENCES

- [1] S. L. McCall, A. F. J. Levi, R. E. Slusher, S. J. Pearson, and R. A. Logan, "Whispering-gallery mode microdisk lasers," *Appl. Phys. Lett.*, vol. 60, no. 3, pp. 289–229, 1992.
- [2] R. E. Slusher, A. F. J. Levi, U. Mohideen, S. L. McCall, S. J. Pearson, and R. A. Logan, "Threshold characteristics of semiconductor microdisk lasers," *Appl. Phys. Lett.*, vol. 63, no. 10, pp. 1310–1312, 1993.
- [3] T. Baba, M. Fujita, M. Kihara, and R. Watanabe, "Lasing characteristics of GaInAsP-InP strained quantum-well microdisk injection lasers with diameter of 2–10 μm ," *IEEE Photon. Technol. Lett.*, vol. 9, no. 7, pp. 878–890, Jul. 1997.
- [4] B. Corbett, J. Justice, L. Considine, S. Walsh, and W. M. Kelly, "Low-threshold lasing in novel microdisk geometries," *IEEE Photon. Technol. Lett.*, vol. 8, no. 7, pp. 855–857, Jul. 1996.
- [5] B. Gayral, J. M. Gerard, A. Lemaitre, C. Dupuis, L. Mamin, and J. L. Pelouard, "High-Q wet-etched GaAs microdisks containing InAs quantum boxes," *Appl. Phys. Lett.*, vol. 75, pp. 1908–1910, 1999.
- [6] H. Cao, J. Y. Xu, W. H. Xiang, Y. Ma, S.-H. Chang, and S. T. Ho, "Optically pumped InAs quantum dot microdisk lasers," *Appl. Phys. Lett.*, vol. 76, no. 24, pp. 3519–3521, 2000.
- [7] M. K. Chin, D. Y. Chu, and S.-T. Ho, "Estimation of the spontaneous emission factor for microdisk lasers via the approximation of whispering gallery modes," *J. Appl. Phys.*, vol. 75, no. 7, pp. 3302–3307, 1994.
- [8] N. C. Frateschi and A. F. J. Levi, "Resonant modes and laser spectrum of microdisk lasers," *Appl. Phys. Lett.*, vol. 66, no. 22, pp. 2932–2934, 1995.
- [9] —, "The spectrum of microdisk lasers," *J. Appl. Phys.*, vol. 80, no. 2, pp. 644–653, 1996.
- [10] G. R. Hadley, "Effective index model for VCSELs," *Opt. Lett.*, vol. 20, pp. 1483–1485, Sep. 1995.
- [11] B.-J. Li and P.-L. Liu, "Numerical analysis of the whispering-gallery modes by the FDTD method," *IEEE J. Quantum Electron.*, vol. 32, no. 9, pp. 1583–1587, Sep. 1996.
- [12] M. Fujita, A. Sakai, and T. Baba, "Ultrasmall and ultralow threshold GaInAsP-InP microdisk injection lasers: design, fabrication, lasing characteristics, and spontaneous emission factor," *IEEE J. Sel. Topics Quantum Electron.*, vol. 5, no. 3, pp. 673–681, May/Jun. 1999.
- [13] O. M. Ramahi, "Stability of absorbing boundary conditions," *IEEE Trans. Antennas Propag.*, vol. 47, no. 4, pp. 593–599, Apr. 1999.
- [14] G. L. Hower *et al.*, "Inaccuracies in numerical calculation of scattering near natural frequencies of penetrable objects," *IEEE Trans. Antennas Propag.*, vol. 41, no. 6, pp. 982–986, Jun. 1993.
- [15] R. P. Wang and M.-M. Dumitrescu, "Theory of optical modes in semiconductor microdisk lasers," *J. Appl. Phys.*, vol. 81, no. 8, pp. 3391–3397, 1997.
- [16] —, "Optical modes in semiconductor microdisk lasers," *IEEE J. Quantum Electron.*, vol. 34, no. 10, pp. 1933–1937, Oct. 1998.
- [17] E. I. Smotrova and A. I. Nosich, "Mathematical analysis of the lasing eigenvalue problem for the WG modes in a 2-D circular dielectric microcavity," *Opt. Quantum Electron.*, vol. 36, no. 1–3, pp. 213–221, 2004.
- [18] M. Abramovitz and I. A. Stegun, *Handbook of Mathematical Functions*. New York: Dover, 1979.
- [19] L. Borruel *et al.*, "Modeling of patterned contacts in tapered lasers," *IEEE J. Quantum Electron.*, vol. 40, no. 10, pp. 1384–1388, Oct. 2004.
- [20] N. B. Rex, R. K. Chang, and L. J. Guido, "Threshold lowering in GaN micropillar lasers by means of spatially selective optical pumping," *IEEE Photon. Technol. Lett.*, vol. 13, no. 1, pp. 1–3, Jan. 2001.
- [21] M. Kneissl, M. Teepe, N. Miyashita, N. M. Johnson, G. D. Chern, and R. K. Chang, "Current-injection spiral-shaped microcavity disk laser diodes with unidirectional emission," *Appl. Phys. Lett.*, vol. 84, no. 14, pp. 2485–2487, 2004.
- [22] S. V. Boriskina, T. M. Benson, P. Sewell, and A. I. Nosich, "Accurate simulation of 2-D optical microcavities with uniquely solvable boundary integral equations and trigonometric Galerkin discretization," *J. Opt. Soc. Amer. A, Opt. Image Sci.*, vol. 21, no. 3, pp. 393–402, 2004.
- [23] D. Colton and R. Kress, *Integral Equation Method in Scattering Theory*. New York: Wiley, 1983.
- [24] S. V. Boriskina, T. M. Benson, P. Sewell, and A. I. Nosich, "Effect of a layered environment on the complex natural frequencies of two-dimensional WGM dielectric ring resonators," *J. Lightwave Technol.*, vol. 20, no. 8, pp. 1563–1572, Aug. 2002.
- [25] A. I. Nosich, "MAR in the wave-scattering and eigenvalue problems: foundations and review of solutions," *IEEE Antennas Propag. Mag.*, vol. 41, no. 3, pp. 34–49, Jun. 1999.
- [26] S. Steinberg, "Meromorphic families of compact operators," *Arch. Rat. Mech. Anal.*, vol. 31, no. 5, pp. 372–379, 1968.



Elena I. Smotrova (S'03) was born in Kharkov, Ukraine, in 1980. She received the M.Sc. degree in applied mathematics from the Kharkov National University, Kharkov, in 2002. She is currently working toward the Ph.D. degree in radio physics at IRE NASU, Kharkov.

Her research interests are in integral equation methods, eigenvalue problems, and semiconductor microcavity laser modeling.

Ms. Smotrova was a recipient of the Young Scientist Prize at the MSMW-04 International Symposium.



Alexander I. Nosich (M'94–SM'95–F'04) was born in Kharkov, Ukraine, in 1953. He earned the M.S., Ph.D., and D.Sc. degrees in radio physics from the Kharkov National University, Kharkov, in 1975, 1979, and 1990, respectively.

Since 1979, he has been with IRE NASU, Kharkov, currently as Leading Scientist. Since 1992, he has held a number of guest fellowships and professorships in the EU, Japan, Singapore, and Turkey. His research interests include the method of analytical regularization for the modeling of open waveguides,

lasers, and antennas.



Trevor M. Benson (M'95–SM'01) was born in Sheffield, Sheffield, U.K., in 1958. He received the B.Sc. degree in physics and the Ph.D. degree in electronic and electrical engineering from the University of Sheffield, Sheffield, in 1979 and 1982, respectively.

From 1983 to 1988, he worked as a Lecturer at University College Cardiff. Since 1989, he has been with the University of Nottingham, Nottingham, U.K., where he became Professor of Optoelectronics in 1996, Director of the Bookham Technology Centre for Optoelectronic Simulation in 2000, and Deputy Director of the George Green Institute for Electromagnetics Research in 2004.

His research interests include numerical and experimental studies of electromagnetic fields, with emphasis on propagation in optical waveguides, modeling of lasers, photonic integrated circuits, and electromagnetic compatibility.



Phillip Sewell (M'91–SM'04) was born in London, U.K., in 1965. He received the B.Sc. and Ph.D. degrees in electronic and electrical engineering from the University of Bath, U.K., in 1988 and 1991, respectively.

In 1991–1993, he was an S.E.R.C. Postdoctoral Fellow at the University of Ancona, Italy. Since 1993, he has been with the University of Nottingham, Nottingham, U.K., now as a Reader. His research interests involve analytical and numerical modeling of electromagnetic problems with application to optoelectronics, microwaves, and electrical machines.